Tunable quantum Mpemba effect in long-range interacting systems

Andrew Hallam,[1,*] Matthew Yusuf,[1,*] Aashish A. Clerk,[2] Ivar Martin,[3,4] and Zlatko Papić[1]
[1]*School of Physics and Astronomy, University of Leeds, Leeds LS2 9JT, United Kingdom*
[2]*Pritzker School of Molecular Engineering, University of Chicago, Chicago, Illinois 60637, USA*
[3]*Materials Science Division, Argonne National Laboratory, Lemont, Illinois 60439, USA*
[4]*Department of Physics, University of Chicago, Chicago, Illinois 60637, USA*

(Received 11 February 2026; revised 24 July 2026; accepted 3 August 2026; published 28 August 2026)

Symmetry plays a fundamental role in many-body systems, both in and out of equilibrium. The quantum Mpemba effect (QME)—a phenomenon where systems initially farther from equilibrium can thermalize faster—can be understood in terms of how rapidly a symmetry, broken by initial conditions, is dynamically restored. In this work, we study the QME in a one-dimensional spin-1/2 XYZ model with power-law decaying interactions in the presence of a magnetic field. In the prethermal regime generated by large field strengths, the system develops a continuous U(1) symmetry, enabling the QME to emerge. However, due to the Hohenberg-Mermin-Wagner theorem, the QME can only arise when interactions are sufficiently short-ranged. This leads to an interplay between the external field, interaction range, and dynamical symmetry restoration. We systematically explore this interplay and analyze the dependence of the QME on the effective temperature set by the initial state. Our results demonstrate the tunability of the QME via long-range interactions, which can be probed in experimental platforms of trapped ions, polar molecules, and NV centers.

DOI: 10.1103/kvth-my1s

I. INTRODUCTION

The notion of spontaneous symmetry breaking (SSB) is central to equilibrium many-body physics. Within the Landau paradigm, phases of matter and transitions between them can be understood by their relationship to the symmetries of the underlying Hamiltonian. Recently, attention has turned to understanding symmetry breaking in nonequilibrium quantum systems. According to the eigenstate thermalization hypothesis (ETH) [1,2], for most Hamiltonians and most initial states, the system is expected to relax to thermal equilibrium [3–5]. Without SSB, the resulting thermal state should be invariant under the symmetries of the system. Therefore, even if the initial state breaks these symmetries, one expects the symmetry to be restored during the time evolution.

Somewhat surprisingly, in many cases it has been found that the *more* symmetry-broken an initial state is, the *more rapid* the symmetry restoration. By analogy with the similar phenomenon in water [6], this behavior has been dubbed the quantum Mpemba effect (QME) [7]. The QME has been predicted in a wide range of systems, including quantum spin chains [8–10], lattice models of fermions and bosons [11,12], quantum circuits [13–19], quantum dots [20,21], and open quantum systems [22–47]. Recently, the QME has also been realized in quantum simulation platforms [48,49]. Most of these works have focused on the restoration of continuous symmetries, in particular, U(1) symmetry associated with particle-number conservation, although systems with non-Abelian SU(2) symmetry have also been shown to exhibit the QME [15,50–52]. In integrable models, the QME arises due to states that are simultaneously more out-of-equilibrium and have larger overlaps with the fastest quasiparticle modes [53]. Similar mechanisms have been used to explain the effect in systems coupled to external reservoirs [54,55]. Recently, Ref. [56] argued that the QME can be generalized to chaotic systems without spatial symmetries or even energy conservation, where there is no quasiparticle description at high energies. This suggests the ubiquity of the QME in quantum many-body systems.

Despite being a nonequilibrium phenomenon, the QME depends upon the eventual restoration of symmetry, and is therefore intimately connected to the system's equilibrium properties. This motivates the question of how the QME and SSB interplay in the context of the Hohenberg-Mermin-Wagner (HMW) theorem [57,58], a celebrated no-go theorem for SSB in spatial dimensions $d \leqslant 2$. One may expect the QME to occur if a phase does not exhibit SSB; conversely, the QME is not expected to persist in a phase with SSB. The existence of SSB can be tuned in systems with long-range (algebraically decaying) interactions [59–64], which can evade the HMW theorem even in $d = 1$. Power-law decaying interactions arise naturally in trapped ions, polar molecules, and NV centers in diamond [65–68] (see also Ref. [62] for a recent overview). In particular, trapped-ion experiments allow the effective decay exponent to be tuned from nearly all-to-all to dipolar regimes by adjusting laser detunings and phonon-mode couplings.

Long-range interactions are a well-known source of unusual nonequilibrium properties, such as suppressed growth of

[*]These authors contributed equally to this work.

Published by the American Physical Society under the terms of the Creative Commons Attribution 4.0 International license. Further distribution of this work must maintain attribution to the author(s) and the published article's title, journal citation, and DOI.

entanglement entropy and dynamical phases of matter [69,70]. This raises a natural question: How does the QME depend on the range of interactions? A recent work [71] investigated signatures of the QME in long-range spin systems using spin-wave analysis and showed that the QME can persist over a range of interaction decay exponents. However, the role of SSB and its implications for dynamical symmetry restoration were not addressed. In particular, it remains unclear whether sufficiently long-range interactions can qualitatively suppress the QME by stabilizing symmetry-broken phases, and how such behavior is modified in systems with only emergent rather than exact continuous symmetries.

Here we study the QME in a one-dimensional (1D) long-range interacting spin-1/2 XYZ chain subject to a longitudinal magnetic field. In the large-field prethermal regime, an emergent U(1) symmetry enables dynamical symmetry restoration, whereas sufficiently long-range interactions promote its SSB. Because our central interest lies in dynamical symmetry restoration, we consider models that do not possess an explicit U(1) symmetry, yet develop an emergent one in the rotating frame at large fields. This approach allows us to capture both symmetry-broken and symmetry-restoring dynamics within a unified framework. By varying the field strength, interaction range, and effective temperature of the initial state, we map out a "QME dynamical phase diagram" and identify the conditions under which the effect halts. These results connect the QME to the HMW theorem and establish tunable routes for its observation in quantum-simulation platforms.

The remainder of this paper is organized as follows. In Sec. II, we introduce the XYZ model and briefly review the physics of its prethermal regime, with an emergent U(1) symmetry and a continuous time crystal phase. This regime will be key to stabilizing the QME. In Sec. II, we also introduce the notion of entanglement asymmetry, ΔS_A, which will be used as the main diagnostic of the QME. Our main results are presented in Secs. III and IV, where we explore two directions in the dynamical phase diagram: varying the strength of the magnetic field and the range of interactions. In Sec. III, we study the effect of varying the magnetic field strength, while in Sec. IV we focus on the large-field regime, studying the effect of U(1) SSB on the QME by varying the interaction range and the energy density of the initial state. The results of Sec. IV directly apply to static systems described by isotropic XXZ Hamiltonians. We summarize our findings in the QME dynamical phase diagram presented in Sec. V, while Supplemental Material (SM) [72] provides further details of trace distance as an alternative measure of the QME, additional numerical results and finite-size scaling analysis, and the study of the SU(2)-symmetric point in the XYZ model.

II. LONG-RANGE XYZ MODEL

Inspired by experimental platforms such as trapped ions and polar molecules [62], we consider a one-dimensional spin-1/2 long-range XYZ spin model in a magnetic field pointing along the z direction, illustrated in Fig. 1(a). The model is defined by the Hamiltonian

$$\hat{H} = \frac{1}{\mathcal{N}} \sum_{i<j} \sum_{\nu\in\{x,y,z\}} \frac{J_\nu}{|i-j|^\alpha} \hat{\sigma}_i^\nu \hat{\sigma}_j^\nu + h_z \sum_i \hat{\sigma}_i^z, \tag{1}$$

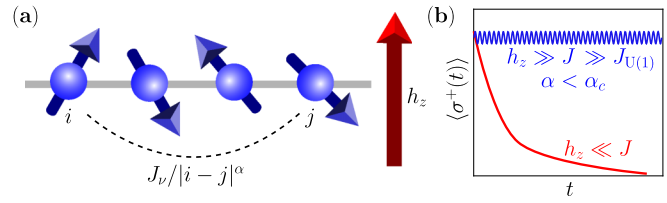


FIG. 1. (a) Schematic of a one-dimensional long-range XYZ spin chain in an external magnetic field h_z. The spins i and j interact via power-law decaying interactions, $(J_\nu/|i-j|^\alpha)\hat{\sigma}_i^\nu\hat{\sigma}_j^\nu$, where J_ν, $\nu = x, y, z$, are the interaction couplings along the three directions and $\hat{\sigma}_i^\nu$ are Pauli matrices, as in Eq. (1). (b) At weak fields, $h_z \ll J_\nu$, there is no U(1) symmetry for generic values of J_ν and the corresponding order parameter, $\sigma^+ \equiv (\sigma^x + i\sigma^y)/2$, rapidly decays to zero as a function of time t. By contrast, in the prethermal regime when $h_z \gg J \gg J_{\mathrm{U}(1)} \equiv |J_x - J_y|$, where J is the largest of the couplings J_ν, the system develops a U(1) symmetry in the rotating frame, accompanied by the persistent nonzero value of $\langle\sigma^+(t)\rangle$—the hallmark of a continuous time crystal [74]. This only occurs when α is smaller than a critical value α_c (see text for details). The goal of this paper is to quantitatively explore the competition between spontaneous symmetry breaking and dynamical symmetry restoration.

where $J_{\nu=x,y,z}$ are the spin-spin couplings, $\hat{\sigma}_i^\nu$ are the standard Pauli matrices on site i, and h_z is the strength of the external magnetic field. The power-law exponent α sets the range of interactions. We assume open boundary conditions for the chain and normalize the spin-spin couplings using the Kac norm [73],

$$\mathcal{N} = \frac{1}{N-1} \sum_{i\neq j} \frac{1}{|i-j|^\alpha}, \tag{2}$$

where N is the total number of spins. This normalization ensures that the energy density is intensive in the thermodynamic limit and allows for a consistent comparison of results at different α.

In the limit $J_x = J_y$, the Hamiltonian reduces to the long-range, U(1)-symmetric XXZ model. When $\alpha \to \infty$, interactions are restricted to nearest neighbors and the model becomes the quantum integrable XXZ spin chain [75]. In the opposite limit $\alpha = 0$, the Hamiltonian is a fully connected Lipkin-Meshkov-Glick (LMG) model [76,77], which can be solved by mapping to a free collective spin [78–80]. However, for any finite α, the model (1) is nonintegrable. Previous studies of ground-state properties at $h_z = 0$ and finite α [61,81] showed that the XXZ model with $J_z \lessapprox 1$ transitions from a gapless, short-range U(1)-preserving XY phase (large α), to a gapless, U(1)-breaking superfluid phase (small α), undergoing a phase transition at a critical $\alpha_c \approx 3$. In the remainder of this section, we focus on the dynamics of the model (1) in the regime of large fields, where it develops an emergent U(1) symmetry and time crystal phase. We also introduce the entanglement asymmetry, which will be used as the main diagnostic of the QME in subsequent sections.

A. Prethermal U(1) symmetry and continuous time crystal

While in equilibrium the model (1) only exhibits U(1) symmetry when $J_x = J_y$, away from equilibrium it is possible to effectively realize U(1) symmetry for generic couplings

J_ν if the field is large, i.e., $h_z \gg J$, where J is the largest of the couplings J_ν. In the rotating frame aligned with the z axis, there is an emergent U(1) symmetry, which can leave dynamical signatures when the system is quenched far from equilibrium, e.g., in the form of a continuous time crystal (CTC) [70,74,82]. We now briefly review this scenario, summarized in Fig. 1(b), as the same regime can be used to create the QME for arbitrary couplings J_ν in Eq. (1), by varying α (and h_z remaining sufficiently large).

According to the static prethermal theorem [83], a Hamiltonian of the form in Eq. (1), i.e., $\hat{H} = \hat{H}_0 + h_z\hat{Z}$, where $\hat{Z} = \sum_i \hat{\sigma}_i^z$ has an integer spectrum, can be transformed (through a series of unitary rotations in the large-h_z limit) into $\hat{D} + \hat{V} + h_z\hat{Z}$, where $\hat{D}$ commutes with $\hat{Z}$ and $\hat{V}$ is an exponentially small correction in h_z. For our model in Eq. (1), this yields [82]

$$\hat{D} = \frac{1}{\mathcal{N}} \sum_{i<j} \frac{J_x + J_y}{2} \left(\frac{\sigma_i^x \sigma_j^x}{|i-j|^\alpha} + \frac{\sigma_i^y \sigma_j^y}{|i-j|^\alpha} \right) + J_z \frac{\sigma_i^z \sigma_j^z}{|i-j|^\alpha}. \tag{3}$$

For timescales that are exponentially long in h_z/J, the dynamics of the model (1) are governed by an effective prethermal Hamiltonian

$$\hat{H}_{\mathrm{XXZ}}^{\mathrm{eff}} \approx \hat{D} + h_z\hat{Z}, \quad \text{valid for} \quad t \ll t_* \sim e^{O(h_z/J)}. \tag{4}$$

This effective Hamiltonian has a U(1) symmetry generated by $\hat{Z}$. Intuitively, Eq. (4) expresses the fact that the large z-magnetic field tends to "homogenize" interactions in the x and y directions in the rotating frame. Note that there are correction terms to Eq. (4) which depend on the explicit U(1)-breaking in the couplings, $J_{\mathrm{U}(1)} \equiv |J_x - J_y|$ [82]. Thus the emergent U(1) symmetry in the prethermal regime is robust provided $h_z \gg J \gg J_{\mathrm{U}(1)}$.

This U(1)-symmetric prethermal regime allows for a rich dynamical phase diagram featuring a CTC phase [82]. The CTC arises under unitary dynamics generated by the effective Hamiltonian (4), hence it is distinct from the more common time crystal realizations in a Floquet setting [84–89], where the couplings of the model are externally modulated and the system breaks a discrete symmetry of the drive [90–94] (for recent reviews of discrete time crystals, see Refs. [95–97]). While in the stationary frame the CTC occurs at a high energy density, in the rotating frame it corresponds to a near-ground state of the effective Hamiltonian (4). Being at a low temperature in the rotating frame, the CTC can develop an order parameter that spontaneously breaks a symmetry. Whether or not SSB occurs in the rotating frame is determined by the range of interactions α.

As discussed above, the ground state of the effective long-range XXZ model (4) exhibits SSB when interactions are sufficiently long-ranged. Dynamically, this manifests as states exhibiting persistent symmetry breaking up to late times. Since the long-range XXZ model is nonintegrable and expected to obey the ETH, whether a particular initial state displays symmetry breaking depends on whether the corresponding finite-temperature Gibbs state also exhibits SSB. For the latter to happen, the couplings J_x and J_y do not necessarily need to be equal to each other, as long as the conditions of the prethermal theorem above hold. What does this imply for the full model (1)? In the limit $h_z \gg J_{\mathrm{U}(1)}$, the h_z field effectively drives rotations in the $x-y$ plane, generating an effective U(1) symmetry. However, the underlying anisotropy in the couplings makes rotations in the $x-y$ plane asymmetric [82], leading to small oscillations in the magnitude of the order parameter of the CTC phase $\langle\sigma^+\rangle$, which are characteristic of a CTC—see Fig. 1(b). On the other hand, when interactions are short-ranged and α is above the SSB transition, the order parameter rapidly decays to $\langle\sigma^+\rangle = 0$, and now the spectrum respects U(1) symmetry, potentially allowing the QME to emerge when considering two different initial states. Before testing this picture in the numerics, we first introduce the definition of the QME used in this work.

B. Entanglement asymmetry as a probe of the QME

The conventional QME setup considers the reduced density matrix $\hat{\rho}_A \equiv \mathrm{Tr}_{\bar{A}}|\psi\rangle\langle\psi|$ over a subset of A spins of a pure state $|\psi\rangle$, where $\mathrm{Tr}_{\bar{A}}$ denotes the partial trace over the complement $\bar{A}$. Crucially, the chosen state $|\psi\rangle$is *not* invariant under some global symmetry generated by an operator $\hat{Q}$. Hence, the symmetry generator restricted to the subsystem, $\hat{Q}_A$, does not commute with $\hat{\rho}_A$:

$$|\psi\rangle \quad \text{obeys} \quad [\hat{\rho}_A, \hat{Q}_A] \neq 0. \tag{5}$$

For simplicity, we will assume $\hat{Q} = \sum_i \hat{\sigma}_i^z$ is the generator of the global U(1) symmetry, such that $\hat{Q}_A = \sum_{i\in A} \hat{\sigma}_i^z$.

To quantify the amount of symmetry breaking in $\hat{\rho}_A$, Ref. [8] introduced a quantity called the *entanglement asymmetry*,

$$\Delta S_A \equiv S(\hat{\rho}_{A,Q}) - S(\hat{\rho}_A), \quad \hat{\rho}_{A,Q} \equiv \sum_{q\in\mathbb{Z}} \hat{\Pi}_q \hat{\rho}_A \hat{\Pi}_q, \tag{6}$$

where $\hat{\Pi}_q$ is the projector onto the eigenspace of $\hat{Q}_A$ with charge $q \in \mathbb{Z}$ and $S(\hat{\rho}) \equiv -\mathrm{Tr}\,\hat{\rho}\ln\hat{\rho}$ is the von Neumann entropy. Generally, we have $\Delta S_A \geqslant 0$ and the equality is attained if and only if $[\hat{\rho}_A, \hat{Q}_A] = 0$. Intuitively, ΔS_A quantifies the norm of the off-diagonal blocks connecting different sectors of $\hat{Q}_A$ in the reduced density matrix $\hat{\rho}_A$.

Using ΔS_A, we are now in a position to define the QME. We will restrict to cases where we prepare the system in translationally invariant states obeying Eq. (5) and parametrized by one or more variables θ (in the simplest case, θ may be the angle of each spin on the Bloch sphere). We will say that the QME occurs if the following two conditions are met:

$$\Delta S_A^{\theta_1}(t=0) > \Delta S_A^{\theta_2}(t=0), \tag{7}$$

$$\Delta S_A^{\theta_1}(t\to\infty) < \Delta S_A^{\theta_2}(t\to\infty). \tag{8}$$

These conditions imply that there is a crossing of the curves $\Delta S_A(t)$ for the two initial states, θ_1 and θ_2. The first crossing $\Delta S_A^{\theta_1}(t{=}\tau_M) = \Delta S_A^{\theta_2}(t{=}\tau_M)$ defines the *Mpemba time*, denoted by τ_M. In the numerical simulations below, it will be convenient to determine τ_M by examining when the ratio of entanglement asymmetries for two states, $\Delta S_A^{\theta_1}/\Delta S_A^{\theta_2}$, drops below unity.

A few comments are in order. First, in contrast to an open quantum system setting [98], in our case the entanglement asymmetry ΔS_A is not necessarily a monotonic function of time. Therefore the asymmetry of two states may exhibit

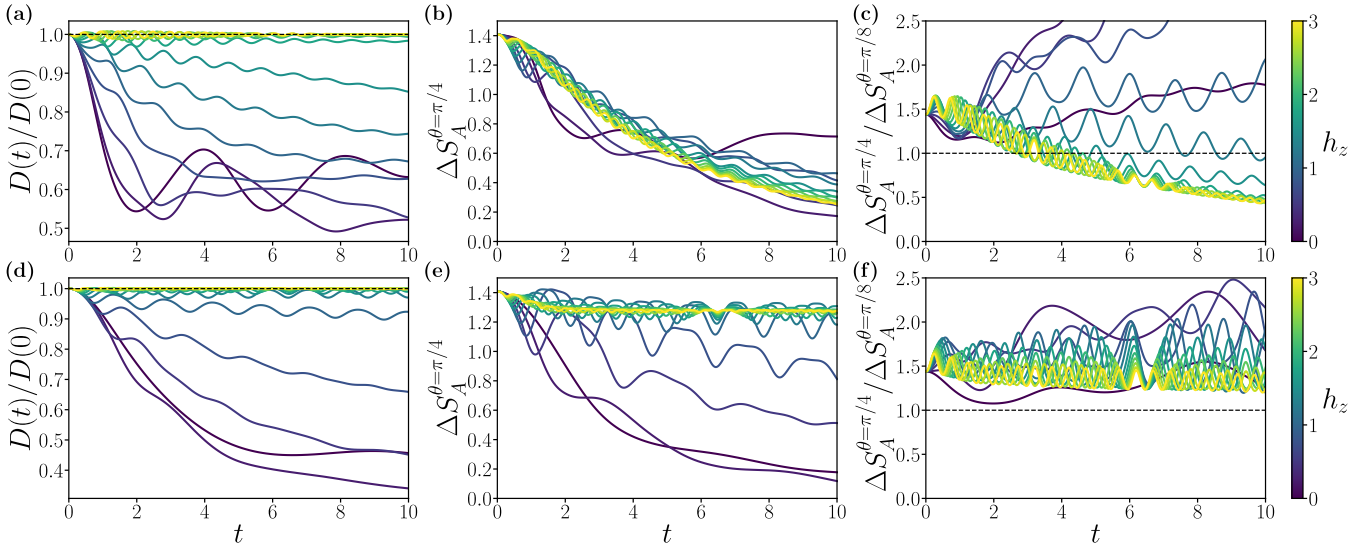


FIG. 2. Quench dynamics for the initial states in Eq. (9) under the long-range XYZ Hamiltonian in Eq. (1). The parameters are $J_x = -0.5$, $J_y = -1.5$, and $J_z = -0.75$, at $\alpha = 4$ (top) and 1.5 (bottom), while the color bar shows the field strength h_z. (a) and (b) show the expectation value $D(t) \equiv \langle\psi(t)|\hat{D}|\psi(t)\rangle$ of the U(1)-invariant effective XXZ Hamiltonian in Eq. (3) for the $\theta = \pi/4$ initial state at $\alpha = 4$ (a) and 1.5 (b). We normalize the curves by $D(t = 0)$. The prethermal regime, $D(t)/D(0) \approx 1$, is seen to be robust for both short- and long-range interactions if the field strength is sufficiently large ($h_z \gtrsim 2$). (c) and (d) show the corresponding entanglement asymmetry ΔS_A for $N_A = 4$ sites for $\alpha = 4$ (c) and 1.5 (d). The symmetry is restored for short-range interactions (c), but not for long-range (d). (e) and (f) show the ratios of the entanglement asymmetry at $\theta_1 = \pi/4$ and $\theta_2 = \pi/8$ at $\alpha = 4$ (e) and 1.5(f). The drop of the large-h_z (red) curves below unity in (e) signals the QME, which is absent for longer-range interactions in (f). All data were obtained for a subsystem of $N_A = 4$ spins in an infinite chain using TDVP with translation-invariant iMPS of bond dimension $\chi = 128$ and a time step $\delta t = 0.025$.

multiple crossings during the evolution. In the cases studied in this paper, we have explicitly verified that the results remain qualitatively unchanged if we define the Mpemba time using the *last* instead of the first crossing. More precisely, while the last crossing can result in a larger Mpemba time, it does not have a strong impact on the interplay between QME and SSB. Second, beyond entanglement asymmetry, we note that there are a number of possible alternative definitions of the QME based on information-theoretic measures of how far a system is from equilibrium, instead of how well the state of the system respects a global symmetry [99]. These measures, such as trace distance [72] and the Frobenius norm, allow one to generalize the notion of the QME to systems without global symmetries [7,56,100–103]. Since our focus is on symmetry breaking and restoration, we adopt the conventional measure, Eq. (6), as a QME diagnostic.

In summary, in the presence of a strong magnetic field and for small differences in transverse spin-spin couplings, the XYZ spin chain is in the robust prethermal regime described by the effective U(1)-symmetric Hamiltonian in Eq. (4). This Hamiltonian undergoes a U(1) SSB transition as the interactions become increasingly long-ranged [59–61]. We conjecture that the occurrence of the QME in this model depends on two conditions: (i) the robustness of the effective XXZ model as the field strength, h_z, is increased, and (ii) the emergence of SSB in the equilibrium XXZ model as the interaction length scale, α^{-1}, is increased. In the following sections, we test this conjecture in numerical simulations. We will detect the QME using the entanglement asymmetry, ΔS_A, for different initial states, where their intersection is identified as the QME.

III. VARYING THE FIELD STRENGTH

We now perform a numerical analysis of the dynamical phase diagram of the model (1) by varying the field strength h_z. We consider quenches from uniformly tilted product initial states:

$$|\psi(t = 0, \theta)\rangle = \bigotimes_j \exp\left(i\theta\hat{\sigma}_j^y\right)|\uparrow\rangle_j, \tag{9}$$

which break the U(1) symmetry (magnetization in the z direction), as prescribed in Eq. (5). We will work in the infinite system-size limit, simulating the dynamics using the time-dependent variational principle (TDVP) for translation-invariant infinite matrix-product states (iMPS) [104–106], approximating the long-range couplings as a sum of exponential terms [107] (see SM [72] for details of our implementation of long-range interactions). Working directly in the thermodynamic limit greatly simplifies the numerical analysis of SSB, since the dynamics in finite systems exhibit $O(N^{1/2})$ system-size-dependent oscillations due to the splitting in the ground-state manifold [108,109] (see SM [72] for a system-size-scaling analysis). For the family of states in Eq. (9), the initial entanglement asymmetry $\Delta S_A(t = 0)$ monotonically increases as θ varies from $\theta = 0$, where $|\psi(t = 0)\rangle = |\uparrow\uparrow\uparrow\ldots\rangle$, to $\theta = \pi/4$, where $|\psi(t = 0)\rangle = |+++\ldots\rangle$.

In Fig. 2, we present quench dynamics for the initial states defined in Eq. (9) and evolved under the long-range XYZ Hamiltonian in Eq. (1) with $J_x = -0.5$, $J_y = -1.5$, and $J_z = -0.75$, at $\alpha = 4$ (upper panels) and $\alpha = 1.5$ (lower panels) for increasing field strength h_z. Figures 2(a) and 2(b) show the expectation value of the prethermal Hamiltonian (3),

$D(t) \equiv \langle\psi(t)|\hat{D}|\psi(t)\rangle$ (normalized by its value at $t = 0$) for the $\theta = \pi/4$ state at $\alpha = 4$ (a) and 1.5 (b). For small h_z, the system rapidly leaves the prethermal regime, as indicated by the sharp drop of $D(t)/D(0)$ below one. In contrast, at large h_z, $D(t)/D(0)$ remains close to one even at late times, demonstrating that the prethermal Hamiltonian accurately captures the dynamics. There are small but noticeable oscillations in $D(t)/D(0)$ as h_z increases. As explained in Sec. II A, these arise because the field drives rotations in the x-y plane, while the asymmetry in the spin-spin couplings in the x and y directions leads to slightly elliptic rotations. These small oscillations are characteristic of the prethermal CTC [82]. It is important to note that this oscillatory behavior is due to subleading corrections to the exact U(1)-symmetric prethermal Hamiltonian in Eq. (4).

Figures 2(c) and 2(d) show the evolution of the entanglement asymmetry ΔS_A for the $\theta = \pi/4$ initial state at $\alpha = 4$ (c) and 1.5 (d). At large h_z, the prethermal phase is robust and there is an emergent U(1) symmetry. As discussed above, when α is large the system is in the U(1)-preserving XY phase, so we expect to observe symmetry restoration. This can be seen in Fig. 2(c) where the entanglement asymmetry tends to 0 for large h_z. In contrast, for $\alpha = 1.5$ the system is in the U(1)-breaking superfluid phase; hence, in Fig. 2(d), the entanglement asymmetry remains constant at late times for large enough h_z.

Altogether, Figs. 2(a)–2(d) serve as a diagnostic of the system being in the prethermal regime, confirming that the quench dynamics matches that of the effective Hamiltonian (3) at large h_z. To directly reveal the QME, in Figs. 2(e) and 2(f), we show the ratio of entanglement asymmetries for two initial states of the form in Eq. (9) with $\theta_1 = \pi/4$ and $\theta_2 = \pi/8$, plotted as a function of time for $\alpha = 4$ and 1.5, respectively. For our choice of parameters, the asymmetry ratio starts out above 1 at $t = 0$, and the QME occurs if it drops below 1 at some later time due to the crossing of the ΔS_A curves traced by the two initial states. At small h_z, for either value of α, the system manifestly breaks U(1) symmetry and, unsurprisingly, we do not observe the ratio dropping below unity, consistent with an absence of the QME. In contrast, at large h_z the emergent U(1) symmetry leads to strikingly different behavior for $\alpha = 4$ compared to $\alpha = 1.5$. For $\alpha = 4$, the U(1)-preserving behavior of the equilibrium physics leads to symmetry restoration in the nonequilibrium dynamics, subsequently leading to the QME in Fig. 2(e). As the field strength decreases and the prethermal timescale of the model becomes shorter, the Mpemba time sharply diverges. For $\alpha = 1.5$, the SSB in the equilibrium model prevents symmetry restoration in the nonequilibrium dynamics, thereby causing the QME to cease, as shown in Fig. 2(f).

To summarize, Fig. 2 demonstrates the correlation between the entanglement asymmetry and the existence of the prethermal Hamiltonian. When h_z is small, the prethermal phase is not robust; therefore there is no emergent U(1) symmetry and dynamical symmetry restoration does not occur, resulting in the absence of a QME. However, when h_z is sufficiently large, the system remains in the prethermal phase where the prethermal XXZ description is valid (due to the prethermalization timescale being sufficiently long). In this regime, symmetry restoration follows the dynamics expected under the prethermal Hamiltonian, where large α implies that the system is in the U(1)-conserving phase leading to dynamical symmetry restoration and the QME, while small α leads to SSB and no symmetry restoration, halting the QME. Thus by tuning h_z and α, the presence of the QME for the class of states in Eq. (9) can be controlled by steering toward or away from symmetry restoration.

IV. TUNING THE INTERACTION RANGE AND ENERGY OF INITIAL STATES

In the previous section, we showed that as h_z increased, the dynamics of the long-range XYZ model in the rotating frame is governed by an effective long-range XXZ model, with qualitatively different behavior for the entanglement asymmetry and QME depending on the value of α. In this section, we work in the $h_z \to \infty$ limit and explicitly study the long-range XXZ model to ascertain the dependence of the QME on α and J_z. We will discuss how the QME depends upon the choice of initial state, in particular the energy density.

Using the tilted product initial states previously introduced in Eq. (9), we analyze the quench dynamics under the XXZ Hamiltonian in Eq. (3) with $J_x = J_y = -1$ and varying α and J_z. Figure 3(a) shows the entanglement asymmetry ratio for $\theta_1 = \pi/4$ and $\theta_2 = \pi/8$ with fixed $J_z = -0.75$ and varying α. Consistent with Figs. 2(e) and 2(f), we notice that increasing the range of interactions halts the QME. Since the long-range XXZ model is nonintegrable, these states are all expected to relax to thermal equilibrium. Therefore the halting of the QME as α is decreased depends on whether the thermal state exhibits SSB or not. This can be quantified using the normalized energy density

$$\epsilon = (E - E_{\min})/(E_{\max} - E_{\min}), \tag{10}$$

where E is the energy of the state, and $E_{\min}$, $E_{\max}$ are those of the lowest and highest energy states, respectively. Larger values of ϵ equilibrate to higher temperature thermal states and consequently require longer interaction ranges to stabilize the U(1) SSB.

The initial states in Eq. (9) are low-energy density states, e.g., we have $\epsilon = 0.003$ for $\theta = \pi/4$ and $\epsilon = 0.068$ for $\theta = \pi/8$ at $J_z = -0.75$ and $\alpha = 2$. However, SSB is expected to occur at smaller α if we consider even higher energy density states. To probe this and access a broader range of ϵ, we consider a class of tilted Néel states:

$$|\varphi(t = 0, \phi)\rangle = \bigotimes_i \Big(|\uparrow\rangle_{2i-1} \otimes [\cos\phi|\uparrow\rangle_{2i} - \sin\phi|\downarrow\rangle_{2i}]\Big). \tag{11}$$

Figure 3(b) shows how the Mpemba time τ_M changes as a function of α for the one-site periodic tilted product initial states in Eq. (9) with $\theta_1 = \pi/4$, $\theta_2 = \pi/8$ (labeled 1-site), and the two-site periodic tilted Néel states in Eq. (11) with $\phi_1 = \pi/4$, $\phi_2 = \pi/8$ (labeled 2-site). For the tilted Néel states, the normalized energy densities are $\epsilon = 0.407$ for $\phi = \pi/4$ and $\epsilon = 0.209$ for $\phi = \pi/8$ at $J_z = -0.75$ and $\alpha = 2$ [72], placing them significantly higher in the spectrum compared to the tilted ferromagnetic states. We find that the Mpemba time for the tilted product states diverges and halts at a shorter range

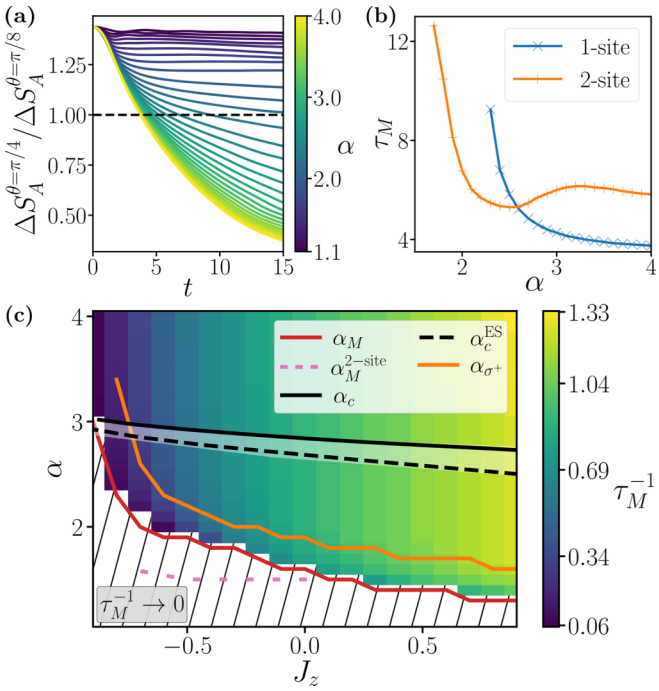


FIG. 3. (a) Ratio of the entanglement asymmetry for the initial states in Eq. (9) with $\theta_1 = \pi/4$ and $\theta_2 = \pi/8$, evolved under the XXZ Hamiltonian (3). Parameters are $J_x = J_y = -1$ and $J_z = -0.75$ with varying α (color bar). (b) The Mpemba time τ_M as a function of α for these states (labeled 1-site), as well as for two tilted Néel states in Eq. (11) with $\phi_1 = \pi/4$ and $\phi_2 = \pi/8$ (labeled 2-site), evolved under the same Hamiltonian. (c) The inverse of the Mpemba time τ_M^{-1} (color bar) as a function of (J_z, α). The red line labeled α_M marks the region where $\tau_M \to \infty$ and no QME occurs for the tilted ferromagnetic states in Eq. (9), while the pink dotted line $\alpha_M^{2-\text{site}}$ denotes the same for the tilted Néel states in Eq. (11) (this line was only computed in the interval $J_z \in [-0.75, 0]$). The SSB phase boundary α_c is defined by central charge c_{eff} deviating from unity by more than 10%. c_{eff} was calculated from finite DMRG comparing the difference in entanglement entropy between system sizes $N = 192$ and 200, following the method in Refs. [59–61], at a maximum bond dimension $\chi = 250$. An alternative estimate of the SSB boundary, α_c^{ES}, was obtained following Ref. [110], where the entanglement spectrum of the ground state was calculated for a system of $N = 192$ spins using DMRG with $\chi = 250$. The shaded area between α_c and α_c^{ES} represents the uncertainty of the SSB boundary. The line α_{σ^+} was obtained by determining the α at which the ratio of the order parameters $\langle\sigma^+\rangle^{\theta=\pi/4}/\langle\sigma^+\rangle^{\theta=\pi/8}$ stays above 1. All dynamics data were obtained for a subsystem of $N_A = 4$ spins using TDVP for iMPS with time step $\delta t = 0.025$ and maximum bond dimension $\chi = 128$.

of interactions than for the tilted Néel states. This is due to the fact that the critical α required to stabilize the U(1) SSB phase decreases with increasing energy density, as the tilted Néel states are expected to thermalize to higher-temperature Gibbs states compared to the tilted ferromagnetic states.

In Fig. 3(c), the extracted Mpemba time τ_M is plotted for a range of (J_z, α) values. The critical line, denoted by α_M, represents the largest value of α for which we do not observe the QME for the tilted ferromagnetic states in Eq. (9). Below this line is a region in which the QME does not occur ($\tau_M \to \infty$). The determined α_M, in principle, depends on the maximum evolution time; however, the plotted value is converged for all J_z values except in the immediate vicinity of $J_z = -1$ [72]. We also calculate $\alpha_M^{2-\text{site}}$, the α at which the QME halts for the tilted Néel states in Eq. (11). We find that it lies below the α_M found for tilted ferromagnetic states, consistent with Fig. 3(b).

This demonstrates that the QME boundary depends on the choice of initial states, with their energy density providing an important tunable parameter. The onset of the QME can also be probed by the order parameter $\langle\sigma^+\rangle$, as shown in Fig. 1(b). Motivated by this, we compute the ratio of $\langle\sigma^+\rangle$ for the $\theta = \pi/4$ and $\theta = \pi/8$ tilted ferromagnetic states, and find that it closely mirrors the corresponding ratio of entanglement asymmetries. This gives us another QME boundary estimate, denoted α_{σ^+} in Fig. 3(c), which serves as an upper bound for α_M. In the special case of subsystem size $N_A = 1$, the two are directly related since the off-diagonal elements of $\hat{\rho}_A$ are proportional to $\langle\sigma^+\rangle$.

An immediate question is how does the α_M critical line compare with the SSB phase boundary? To compare the onset of SSB with the α_M line, we estimated the former using two complementary methods. We determine the location of SSB—denoted by α_c in Fig. 3(b)—following the method in Refs. [59–61] based on the central charge c_{eff} extracted from entanglement entropy scaling in the ground state at a conformally invariant 1D critical point [111,112], obtained from finite-size DMRG using the ITensor library [113,114]. At large values of α, $c_{\text{eff}} = 1$ is quantized due to conformal symmetry [115,116]; as we reduce α, c_{eff} serves as a diagnostic of whether the model has left the XY phase. Eventually, in the SSB phase, c_{eff} is not constrained by conformal symmetry [61,117,118] and can generally deviate from unity. In practice, we find that the SSB phase has a varying c_{eff} that is greater than 1. We therefore define the SSB point by c_{eff} deviating from 1 by more than 10%. As a consistency check, we have used a different method for estimating the SSB point based on the entanglement spectrum [110]. This method produces an alternative estimate of the SSB phase boundary, labeled α_c^{ES} in Fig. 3(b). The two estimates, α_c and α_c^{ES}, are consistent with each other, and the small quantitative differences between them can be viewed as the uncertainty in determining the SSB phase boundary.

Generally, from Fig. 3(c), we infer that $\alpha_M < \alpha_c$; thus U(1) SSB serves as an upper bound for the occurrence of the QME. The physical origin of this separation is that the two boundaries probe different notions of order: α_c is a ground-state property and determines SSB at zero temperature, whereas α_M is a dynamical, state-dependent boundary extracted from finite-energy quenches. If the system thermalizes, the relevant states are characterized by an effective temperature, where SSB is generally less robust than in the ground state. Consequently, longer-range interactions (smaller α) are needed to halt dynamical symmetry restoration, leading naturally to $\alpha_M < \alpha_c$.

This leaves an interesting intermediate regime $\alpha_M < \alpha < \alpha_c$, where the ground state is already ordered, yet the excited states accessed dynamically still permit a finite Mpemba time. Accordingly, the halting of the QME depends on the energy density of the initial states: as the energy density decreases, the line α_M shifts closer to the SSB phase boundary, while

at higher energies the two boundaries move further apart, as confirmed in Fig. 3(b). Even for low-energy product states, a residual separation between α_M and α_c can remain because low energy density does not by itself imply proximity to the correlated ground state. In particular, the product states used here lack the correlations present in the ordered phase, which must first develop dynamically after the quench. Thus the buildup of SSB order can occur on longer timescales than the Mpemba crossing, allowing a finite τ_M even where the ground state is already ordered.

Finally, the discussion above holds away from $J_z = -1$. As J_z approaches $J_z = -1$, a finite Mpemba time cannot be detected within accessible timescales. This is due to the SU(2) symmetry of the $J_z = -1$ point, with the tilted ferromagnetic states of Eq. (9) all becoming exact eigenstates of the Hamiltonian. From this we can infer that as $J_z \to -1$, τ_M will also diverge for $\alpha > \alpha_c$ due to the choice of initial states. Hence, in this limit, the SSB phase boundary no longer bounds the region where the QME will halt, with the QME halting even in the U(1)-conserving region for the tilted ferromagnetic states. In SM [72], we analyze the SU(2) point more closely, finding that the QME with respect to the SU(2) symmetry does not halt, which we attribute to the lack of SU(2) SSB in the ground state of the model.

V. DISCUSSION AND CONCLUSIONS

In this paper, we explored the interplay between the QME and SSB by varying the range of interactions. We analyzed both the full XYZ model and its $h_z \to \infty$ limit, where the dynamics reduce effectively to the XXZ model. We showed that tuning the distance from this limit allows one to control the QME, while in the XXZ limit, SSB can be exploited to suppress the QME by adjusting the interaction range. Finally, we demonstrated that the effective temperature of the initial state plays a crucial role, as the interaction range at which SSB emerges depends sensitively on the state's energy density.

Combining the results of Secs. III and IV, we arrive at a dynamical symmetry-restoration phase diagram in Fig. 4. The QME occurs in the top right corner, corresponding to large fields and sufficiently short-range interactions. This diagram applies to the XYZ model with generally unequal spin–spin couplings in the x and y directions, hence without an explicit U(1) symmetry. A potential caveat of Fig. 4 is its dependence on the choice of initial states. This phase diagram is consistent with our results for the tilted product states (9) and the tilted Néel states (11), while in the SM [72] we demonstrate that similar behavior also holds for random MPS states with bond dimension $\chi = 2$. Thus we expect that a broad class of experimentally preparable initial states follows the dynamical behavior in Fig. 4. Nevertheless, to clearly observe the effect, the initial entanglement-asymmetry ratio must be sufficiently larger than 1.

We note that signatures of the QME have recently been observed in small-scale trapped-ion experiments, which realize the long-range XY spin model [48]. However, Ref. [48] did not explore the effect of SSB or more generic couplings that make the model interacting and break U(1) symmetry. A theoretical investigation of the QME in long-range spin systems was also carried out in Ref. [71] using time-dependent

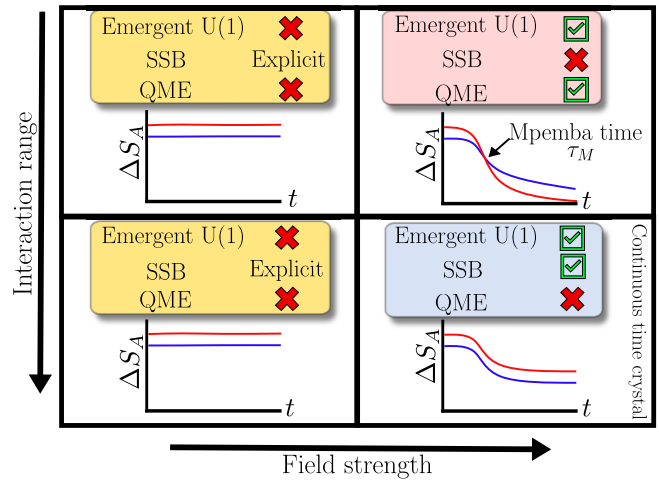


FIG. 4. Dynamical phase diagram of U(1) symmetry restoration in the XYZ model (1) with generic couplings that break the U(1) symmetry, as a function of the field strength h_z and interaction range α. The QME is only possible when the field strength is large, such that the spin couplings become isotropic in the x-y plane, and the U(1) symmetry is preserved because the interactions are effectively short-ranged. We note that this phase diagram is expected to be valid over the prethermal timescale [74], Eq. (4), which depends exponentially on h_z and can be made much longer than the Mpemba time τ_M. Moreover, the phase diagram is, in principle, dependent on the types of initial states, which we assume here to be product states of spins pointing in the same direction on the Bloch sphere [Eq. (9)] or tilted Néel states [Eq. (11)], or their combinations (see text for details).

spin-wave theory, which demonstrated that QME behavior can arise in the semiclassical regime. That work primarily considers finite-size systems and focuses on very long-range interactions ($\alpha < 1$), where symmetry restoration is driven by quantum fluctuations of a precessing ferromagnetic state. Our results address a distinct regime: we work directly in the thermodynamic limit and over a broader range of interaction exponents, where SSB can qualitatively modify the long-time dynamics. In this limit, symmetry need not be restored, and the existence of the QME is sharply tied to whether the system lies in a symmetry-restoring or symmetry-broken phase. This interplay between SSB and dynamical symmetry restoration is essential for understanding when the QME can be suppressed or halted in generic long-range systems with anisotropic interactions.

In this work, we found that an emergent U(1) symmetry could be established using a strong longitudinal field in a Hamiltonian system. Alternatively, U(1) symmetry could arise from Floquet driving, which should lead to analogous behavior for the QME, similar to the prethermal Floquet time-crystal scenario [70,88,89]. Moreover, it would be interesting to study other models that realize SSB of a non-Abelian symmetry. Beyond 1D, the HMW theorem also applies to short-range interacting systems in $d = 2$ spatial dimensions, but can be evaded using sufficiently long-range algebraic interactions. Therefore we expect a similar halting of the QME in models such as the long-range spin-1/2 Heisenberg model in $d = 2$ as the length scale of interactions is tuned [119].

By contrast, in $d = 3$ SSB becomes possible even with short-range interactions, hence it would be particularly interesting to explore the interplay with the QME in this case. While this is challenging for classical numerics, it would be a suitable task for quantum simulations as the relatively short Mpemba time makes the problem amenable to the current generation of noisy quantum hardware.

ACKNOWLEDGMENTS

We would like to thank T. Bhore and J. Ren for useful discussions. We acknowledge the use of the ITensor library [113,114] for the DMRG calculations presented in this work. We acknowledge support by the Leverhulme Trust Research Leadership Award No. RL-2019-015 and EPSRC Grants No. EP/Z533634/1, No. EP/W524372/1, No. UKRI1337, and No. UKRI3780. This research was supported in part by grant NSF Grant No. PHY-2309135 to the Kavli Institute for Theoretical Physics (KITP). Z.P. acknowledges support by the Erwin Schrödinger International Institute for Mathematics and Physics. I.M. acknowledges support by the U.S. Department of Energy, Office of Science, Basic Energy Sciences, Materials Sciences and Engineering Division.

DATA AVAILABILITY

The data that support the findings of this article are openly available [120].

[1] J. M. Deutsch, Quantum statistical mechanics in a closed system, Phys. Rev. A **43**, 2046 (1991).
[2] M. Srednicki, Chaos and quantum thermalization, Phys. Rev. E **50**, 888 (1994).
[3] M. Rigol, V. Dunjko, and M. Olshanii, Thermalization and its mechanism for generic isolated quantum systems, Nature (London) **452**, 854 (2008).
[4] L. D'Alessio, Y. Kafri, A. Polkovnikov, and M. Rigol, From quantum chaos and eigenstate thermalization to statistical mechanics and thermodynamics, Adv. Phys. **65**, 239 (2016).
[5] M. Ueda, Quantum equilibration, thermalization and prethermalization in ultracold atoms, Nat. Rev. Phys. **2**, 669 (2020).
[6] E. B. Mpemba and D. G. Osborne, Cool? Phys. Educ. **4**, 172 (1969).
[7] F. Ares, P. Calabrese, and S. Murciano, The quantum Mpemba effects, Nat. Rev. Phys. **7**, 451 (2025).
[8] F. Ares, S. Murciano, and P. Calabrese, Entanglement asymmetry as a probe of symmetry breaking, Nat. Commun. **14**, 2036 (2023).
[9] S. Murciano, F. Ares, I. Klich, and P. Calabrese, Entanglement asymmetry and quantum Mpemba effect in the XY spin chain, J. Stat. Mech.: Theory Exp. (2024) 013103.
[10] S. Liu, H.-K. Zhang, S. Yin, S.-X. Zhang, and H. Yao, Quantum Mpemba effects in many-body localization systems, Sci. Bull. **70**, 3991 (2025).
[11] S. Yamashika, F. Ares, and P. Calabrese, Entanglement asymmetry and quantum Mpemba effect in two-dimensional free-fermion systems, Phys. Rev. B **110**, 085126 (2024).
[12] S. Yamashika, P. Calabrese, and F. Ares, Quenching from superfluid to free bosons in two dimensions: Entanglement, symmetries, and the quantum Mpemba effect, Phys. Rev. A **111**, 043304 (2025).
[13] F. Ares, S. Murciano, P. Calabrese, and L. Piroli, Entanglement asymmetry dynamics in random quantum circuits, Phys. Rev. Res. **7**, 033135 (2025).
[14] H. Yu, Z.-X. Li, and S.-X. Zhang, Symmetry breaking dynamics in quantum many-body systems, Chin. Phys. Lett. **42**, 110602 (2025).
[15] S. Liu, H.-K. Zhang, S. Yin, and S.-X. Zhang, Symmetry restoration and quantum Mpemba effect in symmetric random circuits, Phys. Rev. Lett. **133**, 140405 (2024).
[16] X. Turkeshi, P. Calabrese, and A. De Luca, Quantum Mpemba effect in random circuits, Phys. Rev. Lett. **135**, 040403 (2025).
[17] K. Klobas, C. Rylands, and B. Bertini, Translation symmetry restoration under random unitary dynamics, Phys. Rev. B **111**, L140304 (2025).
[18] K. Klobas, Non-equilibrium dynamics of symmetry-resolved entanglement and entanglement asymmetry: Exact asymptotics in Rule 54, J. Phys. A: Math. Theor. **57**, 505001 (2024).
[19] A. Foligno, P. Calabrese, and B. Bertini, Nonequilibrium dynamics of charged dual-unitary circuits, PRX Quantum **6**, 010324 (2025).
[20] J. Graf, J. Splettstoesser, and J. Monsel, Role of electron–electron interaction in the Mpemba effect in quantum dots, J. Phys.: Condens. Matter **37**, 195302 (2025).
[21] K. Zatsarynna, A. Nava, R. Egger, and A. Zazunov, Green's function approach to Josephson dot dynamics and application to quantum Mpemba effects, Phys. Rev. B **111**, 104506 (2025).
[22] F. Carollo, A. Lasanta, and I. Lesanovsky, Exponentially accelerated approach to stationarity in Markovian open quantum systems through the Mpemba effect, Phys. Rev. Lett. **127**, 060401 (2021).
[23] J. Zhang, G. Xia, C.-W. Wu, T. Chen, Q. Zhang, Y. Xie, W.-B. Su, W. Wu, C.-W. Qiu, P.-X. Chen, W. Li, H. Jing, and Y.-L. Zhou, Observation of quantum strong Mpemba effect, Nat. Commun. **16**, 301 (2025).
[24] S. Kochsiek, F. Carollo, and I. Lesanovsky, Accelerating the approach of dissipative quantum spin systems towards stationarity through global spin rotations, Phys. Rev. A **106**, 012207 (2022).
[25] R. Bao and Z. Hou, Accelerating relaxation in Markovian open quantum systems through quantum reset processes, Phys. Rev. Lett. **135**, 150403 (2025).
[26] F. Ivander, N. Anto-Sztrikacs, and D. Segal, Hyperacceleration of quantum thermalization dynamics by bypassing long-lived coherences: An analytical treatment, Phys. Rev. E **108**, 014130 (2023).
[27] Y.-L. Zhou, X.-D. Yu, C.-W. Wu, X.-Q. Li, J. Zhang, W. Li, and P.-X. Chen, Accelerating relaxation through Liouvillian exceptional point, Phys. Rev. Res. **5**, 043036 (2023).
[28] A. K. Chatterjee, S. Takada, and H. Hayakawa, Quantum Mpemba effect in a quantum dot with reservoirs, Phys. Rev. Lett. **131**, 080402 (2023).
[29] X. Wang and J. Wang, Mpemba effects in nonequilibrium open quantum systems, Phys. Rev. Res. **6**, 033330 (2024).

[30] D. Liu, J. Yuan, H. Ruan, Y. Xu, S. Luo, J. He, X. He, Y. Ma, and J. Wang, Speeding up quantum heat engines by the Mpemba effect, Phys. Rev. A **110**, 042218 (2024).
[31] S. Longhi, Photonic Mpemba effect, Opt. Lett. **49**, 5188 (2024).
[32] X. Wang, J. Su, and J. Wang, Thermalization and Mpemba-like patterns in effective temperature dynamics of strongly coupled dissipative quantum chaotic systems, Phys. Rev. B **113**, 045119 (2026).
[33] J. Furtado and A. C. Santos, Enhanced quantum Mpemba effect with squeezed thermal reservoirs, Ann. Phys. **480**, 170135 (2025).
[34] D. Qian, H. Wang, and J. Wang, Intrinsic quantum Mpemba effect in Markovian systems and quantum circuits, Phys. Rev. B **111**, L220304 (2025).
[35] L. P. Bettmann and J. Goold, Information geometry approach to quantum stochastic thermodynamics, Phys. Rev. E **111**, 014133 (2025).
[36] J. W. Dong, H. F. Mu, M. Qin, and H. T. Cui, Quantum Mpemba effect of localization in the dissipative mosaic model, Phys. Rev. A **111**, 022215 (2025).
[37] A. Nava and R. Egger, Mpemba effects in open nonequilibrium quantum systems, Phys. Rev. Lett. **133**, 136302 (2024).
[38] I. Medina, O. Culhane, F. C. Binder, G. T. Landi, and J. Goold, Anomalous discharging of quantum batteries: The ergotropic Mpemba effect, Phys. Rev. Lett. **134**, 220402 (2025).
[39] F. Kheirandish, N. Cheraghpour, and A. Moradian, The Mpemba effect in quantum oscillating and two-level systems, Phys. Lett. A **559**, 130915 (2025).
[40] D. J. Strachan, A. Purkayastha, and S. R. Clark, Non-Markovian quantum Mpemba effect, Phys. Rev. Lett. **134**, 220403 (2025).
[41] Z.-M. Wang, S. L. Wu, M. S. Byrd, and L.-A. Wu, Going beyond quantum Markovianity and back to reality: An exact master equation study, arXiv:2411.17197.
[42] S. Mondal and U. Sen, Mpemba effect in self-contained quantum refrigerators: Accelerated cooling, Phys. Rev. A **113**, 022211 (2026).
[43] W. Ma and J. Liu, Quantum Mpemba effect in parity-time symmetric systems, Phys. Rev. B **112**, 214310 (2025).
[44] Z. Wei, M. Xu, X.-P. Jiang, H. Hu, and L. Pan, Quantum Mpemba effect in dissipative spin chains at criticality, Science China Physics, Mechanics & Astronomy **69**, 240315 (2026).
[45] A. Ali, M. I. Hussain, H. A. Zad, H. Kuniyil, M. T. Rahim, S. Al-Kuwari, and S. Haddadi, Quantum Mpemba effect in a four-site Bose-Hubbard model, Fortschr. Phys. **74**, e70089 (2026).
[46] Y. Li, W. Li, and X. Li, Ergotropic Mpemba effect in non-Markovian quantum systems, Phys. Rev. A **112**, 032209 (2025).
[47] A. Chatterjee, S. Khan, S. Jain, and T. S. Mahesh, Direct experimental observation of quantum Mpemba effect without bath engineering, arXiv:2509.13451.
[48] L. K. Joshi, J. Franke, A. Rath, F. Ares, S. Murciano, F. Kranzl, R. Blatt, P. Zoller, B. Vermersch, P. Calabrese, C. F. Roos, and M. K. Joshi, Observing the quantum Mpemba effect in quantum simulations, Phys. Rev. Lett. **133**, 010402 (2024).
[49] Y. Xu, C.-P. Fang, B.-J. Chen, M.-C. Wang, Z.-Y. Ge, Y.-H. Shi, Y. Liu, C.-L. Deng, K. Zhao, Z.-H. Liu, T.-M. Li, H. Li, Z. Wang, G.-H. Liang, D. Feng, X. Guo, X.-Y. Gu, Y. He, H.-T. Liu, Z.-Y. Mei, *et al.*, Observation and modulation of the quantum Mpemba effect on a superconducting quantum processor, Phys. Rev. Lett. **137**, 010402 (2026).
[50] C. Rylands, E. Vernier, and P. Calabrese, Dynamical symmetry restoration in the Heisenberg spin chain, J. Stat. Mech.: Theory Exp. (2024) 123102.
[51] H. Yu, S. Liu, and S.-X. Zhang, Quantum Mpemba effects from symmetry perspectives, AAPPS Bull. **35**, 17 (2025).
[52] H. Fujimura and S. Shimamori, Entanglement asymmetry and quantum Mpemba effect for non-Abelian global symmetry, J. High Energy Phys. 03 (2026) 244.
[53] C. Rylands, K. Klobas, F. Ares, P. Calabrese, S. Murciano, and B. Bertini, Microscopic origin of the quantum Mpemba effect in integrable systems, Phys. Rev. Lett. **133**, 010401 (2024).
[54] F. Ares, V. Vitale, and S. Murciano, Quantum Mpemba effect in free-fermionic mixed states, Phys. Rev. B **111**, 104312 (2025).
[55] F. Caceffo, S. Murciano, and V. Alba, Entangled multiplets, asymmetry, and quantum Mpemba effect in dissipative systems, J. Stat. Mech.: Theory Exp. (2024) 063103.
[56] T. Bhore, L. Su, I. Martin, A. A. Clerk, and Z. Papić, Quantum Mpemba effect without global symmetries, Phys. Rev. B **112**, L121109 (2025).
[57] N. D. Mermin and H. Wagner, Absence of ferromagnetism or antiferromagnetism in one- or two-dimensional isotropic Heisenberg models, Phys. Rev. Lett. **17**, 1133 (1966).
[58] P. C. Hohenberg, Existence of long-range order in one and two dimensions, Phys. Rev. **158**, 383 (1967).
[59] Z.-X. Gong, M. F. Maghrebi, A. Hu, M. Foss-Feig, P. Richerme, C. Monroe, and A. V. Gorshkov, Kaleidoscope of quantum phases in a long-range interacting spin-1 chain, Phys. Rev. B **93**, 205115 (2016).
[60] Z.-X. Gong, M. F. Maghrebi, A. Hu, M. L. Wall, M. Foss-Feig, and A. V. Gorshkov, Topological phases with long-range interactions, Phys. Rev. B **93**, 041102(R) (2016).
[61] M. F. Maghrebi, Z.-X. Gong, and A. V. Gorshkov, Continuous symmetry breaking in 1D long-range interacting quantum systems, Phys. Rev. Lett. **119**, 023001 (2017).
[62] N. Defenu, T. Donner, T. Macrì, G. Pagano, S. Ruffo, and A. Trombettoni, Long-range interacting quantum systems, Rev. Mod. Phys. **95**, 035002 (2023).
[63] C. Chen, G. Bornet, M. Bintz, G. Emperauger, L. Leclerc, V. S. Liu, P. Scholl, D. Barredo, J. Hauschild, S. Chatterjee, M. Schuler, A. M. Läuchli, M. P. Zaletel, T. Lahaye, N. Y. Yao, and A. Browaeys, Continuous symmetry breaking in a two-dimensional Rydberg array, Nature (London) **616**, 691 (2023).
[64] L. Feng, O. Katz, C. Haack, M. Maghrebi, A. V. Gorshkov, Z. Gong, M. Cetina, and C. Monroe, Continuous symmetry breaking in a trapped-ion spin chain, Nature (London) **623**, 713 (2023).
[65] C. Gross and I. Bloch, Quantum simulations with ultracold atoms in optical lattices, Science **357**, 995 (2017).
[66] F. Schäfer, T. Fukuhara, S. Sugawa, Y. Takasu, and Y. Takahashi, Tools for quantum simulation with ultracold atoms in optical lattices, Nat. Rev. Phys. **2**, 411 (2020).
[67] J. Choi, H. Zhou, H. S. Knowles, R. Landig, S. Choi, and M. D. Lukin, Robust dynamic Hamiltonian engineering of many-body spin systems, Phys. Rev. X **10**, 031002 (2020).

[68] H. Zhou, J. Choi, S. Choi, R. Landig, A. M. Douglas, J. Isoya, F. Jelezko, S. Onoda, H. Sumiya, P. Cappellaro, H. S. Knowles, H. Park, and M. D. Lukin, Quantum metrology with strongly interacting spin systems, Phys. Rev. X **10**, 031003 (2020).

[69] A. Lerose and S. Pappalardi, Origin of the slow growth of entanglement entropy in long-range interacting spin systems, Phys. Rev. Res. **2**, 012041(R) (2020).

[70] F. Machado, D. V. Else, G. D. Kahanamoku-Meyer, C. Nayak, and N. Y. Yao, Long-range prethermal phases of nonequilibrium matter, Phys. Rev. X **10**, 011043 (2020).

[71] S. Yamashika and F. Ares, The quantum Mpemba effect in long-range spin systems, Phys. Rev. Lett. **136**, 090402 (2026).

[72] See Supplemental Material at http://link.aps.org/supplemental/10.1103/kvth-my1s for further details and numerical results.

[73] M. Kac, G. E. Uhlenbeck, and P. C. Hemmer, On the van der Waals theory of the vapor-liquid equilibrium. I. Discussion of a one-dimensional model, J. Math. Phys. **4**, 216 (1963).

[74] D. V. Else, B. Bauer, and C. Nayak, Prethermal phases of matter protected by time-translation symmetry, Phys. Rev. X **7**, 011026 (2017).

[75] B. Sutherland, *Beautiful Models 70 Years of Exactly Solved Quantum Many-Body Problems* (World Scientific Publishing Company, River Edge, NJ, 2004).

[76] H. Lipkin, N. Meshkov, and A. Glick, Validity of many-body approximation methods for a solvable model: (i). Exact solutions and perturbation theory, Nucl. Phys. **62**, 188 (1965).

[77] N. Meshkov, A. Glick, and H. Lipkin, Validity of many-body approximation methods for a solvable model: (ii). Linearization procedures, Nucl. Phys. **62**, 199 (1965).

[78] B. Sciolla and G. Biroli, Quantum quenches and off-equilibrium dynamical transition in the infinite-dimensional Bose-Hubbard model, Phys. Rev. Lett. **105**, 220401 (2010).

[79] B. Sciolla and G. Biroli, Quantum quenches, dynamical transitions, and off-equilibrium quantum criticality, Phys. Rev. B **88**, 201110(R) (2013).

[80] A. Lerose and S. Pappalardi, Bridging entanglement dynamics and chaos in semiclassical systems, Phys. Rev. A **102**, 032404 (2020).

[81] J. Ren, W.-L. You, and X. Wang, Entanglement and correlations in a one-dimensional quantum spin-$\frac{1}{2}$ chain with anisotropic power-law long-range interactions, Phys. Rev. B **101**, 094410 (2020).

[82] K. Bull, A. Hallam, Z. Papić, and I. Martin, Tuning between continuous time crystals and many-body scars in long-range XYZ spin chains, Phys. Rev. Lett. **129**, 140602 (2022).

[83] D. Abanin, W. De Roeck, W. W. Ho, and F. Huveneers, A rigorous theory of many-body prethermalization for periodically driven and closed quantum systems, Commun. Math. Phys. **354**, 809 (2017).

[84] S. Choi, J. Choi, R. Landig, G. Kucsko, H. Zhou, J. Isoya, F. Jelezko, S. Onoda, H. Sumiya, V. Khemani, C. von Keyserlingk, N. Y. Yao, E. Demler, and M. D. Lukin, Observation of discrete time-crystalline order in a disordered dipolar many-body system, Nature (London) **543**, 221 (2017).

[85] J. Zhang, P. W. Hess, A. Kyprianidis, P. Becker, A. Lee, J. Smith, G. Pagano, I.-D. Potirniche, A. C. Potter, A. Vishwanath, N. Y. Yao, and C. Monroe, Observation of a discrete time crystal, Nature (London) **543**, 217 (2017).

[86] J. Randall, C. E. Bradley, F. V. van der Gronden, A. Galicia, M. H. Abobeih, M. Markham, D. J. Twitchen, F. Machado, N. Y. Yao, and T. H. Taminiau, Many-body localized discrete time crystal with a programmable spin-based quantum simulator, Science **374**, 1474 (2021).

[87] X. Mi, M. Ippoliti, C. Quintana, A. Greene, Z. Chen, J. Gross, F. Arute, K. Arya, J. Atalaya, R. Babbush, J. C. Bardin, J. Basso, A. Bengtsson, A. Bilmes, A. Bourassa, L. Brill, M. Broughton, B. B. Buckley, D. A. Buell, B. Burkett, *et al.*, Time-crystalline eigenstate order on a quantum processor, Nature (London) **601**, 531 (2022).

[88] A. Kyprianidis, F. Machado, W. Morong, P. Becker, K. S. Collins, D. V. Else, L. Feng, P. W. Hess, C. Nayak, G. Pagano, N. Y. Yao, and C. Monroe, Observation of a prethermal discrete time crystal, Science **372**, 1192 (2021).

[89] W. Beatrez, C. Fleckenstein, A. Pillai, E. de Leon Sanchez, A. Akkiraju, J. Diaz Alcala, S. Conti, P. Reshetikhin, E. Druga, M. Bukov, and A. Ajoy, Critical prethermal discrete time crystal created by two-frequency driving, Nat. Phys. **19**, 407 (2023).

[90] V. Khemani, A. Lazarides, R. Moessner, and S. L. Sondhi, Phase structure of driven quantum systems, Phys. Rev. Lett. **116**, 250401 (2016).

[91] D. V. Else, B. Bauer, and C. Nayak, Floquet time crystals, Phys. Rev. Lett. **117**, 090402 (2016).

[92] C. W. von Keyserlingk, V. Khemani, and S. L. Sondhi, Absolute stability and spatiotemporal long-range order in Floquet systems, Phys. Rev. B **94**, 085112 (2016).

[93] N. Y. Yao, A. C. Potter, I.-D. Potirniche, and A. Vishwanath, Discrete time crystals: Rigidity, criticality, and realizations, Phys. Rev. Lett. **118**, 030401 (2017).

[94] W. W. Ho, S. Choi, M. D. Lukin, and D. A. Abanin, Critical time crystals in dipolar systems, Phys. Rev. Lett. **119**, 010602 (2017).

[95] K. Sacha and J. Zakrzewski, Time crystals: A review, Rep. Prog. Phys. **81**, 016401 (2018).

[96] V. Khemani, R. Moessner, and S. L. Sondhi, A brief history of time crystals, arXiv:1910.10745.

[97] D. V. Else, C. Monroe, C. Nayak, and N. Y. Yao, Discrete time crystals, Annu. Rev. Condens. Matter Phys. **11**, 467 (2020).

[98] Z. Lu and O. Raz, Nonequilibrium thermodynamics of the Markovian Mpemba effect and its inverse, Proc. Natl. Acad. Sci. USA **114**, 5083 (2017).

[99] A. Summer, M. Moroder, L. P. Bettmann, X. Turkeshi, I. Marvian, and J. Goold, A resource theoretical unification of Mpemba effects: Classical and quantum, Phys. Rev. X **16**, 011065 (2026).

[100] F. Ares, C. Rylands, and P. Calabrese, A simpler probe of the quantum Mpemba effect in closed systems, J. Phys. A: Math. Theor. **58**, 445302 (2025).

[101] G. Sreejith and S. Manna, Signatures of quantum chaos and complexity in the Ising model on random graphs, Phys. Rev. B **113**, 214322 (2026).

[102] G. Parez and V. Alba, Reduced fidelities for free fermions out of equilibrium: From dynamical quantum phase transitions to Mpemba effect, J. Stat. Mech. (2026) 013103.

[103] S. Yamashika, S. Endo, and H. Tajima, Quantum Fisher information as a measure of symmetry breaking in quantum many-body systems, arXiv:2509.07468.

[104] J. Haegeman, J. I. Cirac, T. J. Osborne, I. Pižorn, H. Verschelde, and F. Verstraete, Time-dependent variational principle for quantum lattices, Phys. Rev. Lett. **107**, 070601 (2011).

[105] J. Haegeman, C. Lubich, I. Oseledets, B. Vandereycken, and F. Verstraete, Unifying time evolution and optimization with matrix product states, Phys. Rev. B **94**, 165116 (2016).

[106] L. Vanderstraeten, J. Haegeman, and F. Verstraete, Tangent-space methods for uniform matrix product states, SciPost Phys. Lect. Notes, 7 (2019).

[107] B. Pirvu, V. Murg, J. I. Cirac, and F. Verstraete, Matrix product operator representations, New J. Phys. **12**, 025012 (2010).

[108] P. W. Anderson, An approximate quantum theory of the antiferromagnetic ground state, Phys. Rev. **86**, 694 (1952).

[109] H. Tasaki, Long-range order, "tower" of states, and symmetry breaking in lattice quantum systems, J. Stat. Phys. **174**, 735 (2019).

[110] J. T. Schneider, S. J. Thomson, and L. Sanchez-Palencia, Entanglement spectrum and quantum phase diagram of the long-range XXZ chain, Phys. Rev. B **106**, 014306 (2022).

[111] P. Calabrese and J. Cardy, Entanglement entropy and quantum field theory, J. Stat. Mech.: Theory Exp. (2004) P06002.

[112] P. Calabrese and J. Cardy, Entanglement entropy and conformal field theory, J. Phys. A: Math. Theor. **42**, 504005 (2009).

[113] M. Fishman, S. R. White, and E. M. Stoudenmire, The ITensor software library for tensor network calculations, SciPost Phys. Codebases 4 (2022).

[114] M. Fishman, S. R. White, and E. M. Stoudenmire, Codebase release 0.3 for ITensor, SciPost Phys. Codebases 4-r0.3 (2022).

[115] F. C. Alcaraz and A. Moreo, Critical behavior of anisotropic spin-s Heisenberg chains, Phys. Rev. B **46**, 2896 (1992).

[116] S. Ejima and H. Fehske, Comparative density-matrix renormalization group study of symmetry-protected topological phases in spin-1 chain and Bose-Hubbard models, Phys. Rev. B **91**, 045121 (2015).

[117] D. Vodola, L. Lepori, E. Ercolessi, A. V. Gorshkov, and G. Pupillo, Kitaev chains with long-range pairing, Phys. Rev. Lett. **113**, 156402 (2014).

[118] D. Vodola, L. Lepori, E. Ercolessi, and G. Pupillo, Long-range Ising and Kitaev models: Phases, correlations and edge modes, New J. Phys. **18**, 015001 (2015).

[119] J. Zhao, M. Song, Y. Qi, J. Rong, and Z. Y. Meng, Finite-temperature critical behaviors in 2D long-range quantum Heisenberg model, npj Quantum Mater. **8**, 59 (2023).

[120] A. Hallam, M. Yusuf, A. A. Clerk, I. Martin, and Z. Papić, 10.5518/1825.